

Chapter 8

Solar Radiation Interpolation



Ana M. Martín and Javier Dominguez

Abstract Geographic information systems provide different options to analyze and represent the spatial heterogeneity of solar radiation incident on a certain area. This chapter presents a description of the main and well-known methods for determining interpolation surfaces from a data sample. Moreover, using 3D model of the analyzed area, computer models of spatial analysis are precise techniques to adjust the results to the variability of surfaces in a geographic area. Both alternatives offer a great analysis capacity. The selection of a procedure will depend on the objective of the study and the available information.

1 Introduction

Studies about the amount of solar radiation that reaches a surface are of great importance in various areas such as agriculture, ecology, hydrology, biology, meteorology, architecture or the use of solar energy as an alternative for energy supply. The use of solar energy is conditioned by the intensity of the incident solar radiation, so that it is essentially an adequate knowledge of the solar resource distribution.

Although there are solar radiation maps for large geographic areas, in some detailed project solar radiation data are required. In this cases, where there are not measuring stations, will be needed to approximate the data. Sometimes, they can assume as a valid value, the nearest station data and others can use these measurements, using spatial interpolation techniques, to analyze and model the solar resource in no data locations within the same area.

A. M. Martín · J. Dominguez (✉)
Renewable Energy Division (Energy Department) of CIEMAT,
Avda Complutense 40, 28040 Madrid, Spain
e-mail: javier.dominguez@ciemat.es

A. M. Martín
e-mail: AnaMaria.Martin@externos.ciemat.es

© Springer Nature Switzerland AG 2019
J. Polo et al. (eds.), *Solar Resources Mapping*, Green Energy and Technology,
https://doi.org/10.1007/978-3-319-97484-2_8

221

If there are few measuring stations or the installed network is not dense enough, the addition of data from remote sensors, such as satellite images will improve the adjustment of the estimations. Another alternative to calculate the solar radiation is the use of models included in geographic information systems (GIS) software. These systems incorporate the option of evaluating the influence of elevation, considering the geospatial variations of solar radiation between areas of more and less complex relief.

The purpose of this chapter is to feature the capacity of this type of tools in the determination of solar radiation for a specific geographical area. First, the main interpolation methods will be summarized and then, one of the existing GIS models will be described for the estimation of solar radiation considering the influence of terrain topography.

2 Interpolation of Solar Radiation Data Using GIS

The values obtained by interpolation process would depend on the characteristics of the studied geographical variables, the available sample, factors associated with the distribution of the data, the required spatial resolution and the chosen predictor model (Burrough and McDonnell 1998). In general, interpolation techniques are classified as deterministic and geostatistical (Johnston et al. 2001; Santos Preciado and García Lázaro 2008).

The *deterministic techniques* create interpolated surfaces based on the adjustment of mathematical functions to the measured points. They define a set of explanatory variables so that the errors were minimal.

The *geostatistical techniques* generate the prediction surfaces using statistical models. These methods quantify the spatial correlation of the data and evaluate the uncertainty of the obtained results.

In addition, interpolation methods are classified as exact and inexact. They are considered exact when the interpolated values for a location correspond to the measured data (Fig. 1). Finally, they are divided into global and local methods. Global interpolations use a single function to create the continuous surface from all the sample values and, local interpolations adjust the function to different small areas of the sample points. Local methods are more appropriate when the total trend of the analyzed data is unknown (Fig. 2).

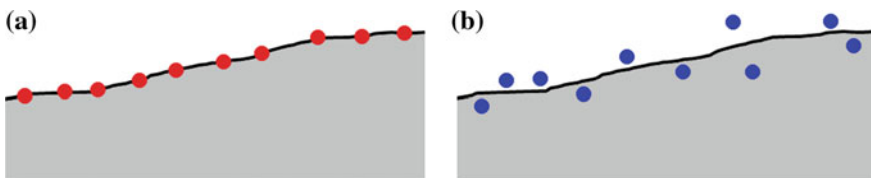


Fig. 1 a Exact and b inexact interpolation methods

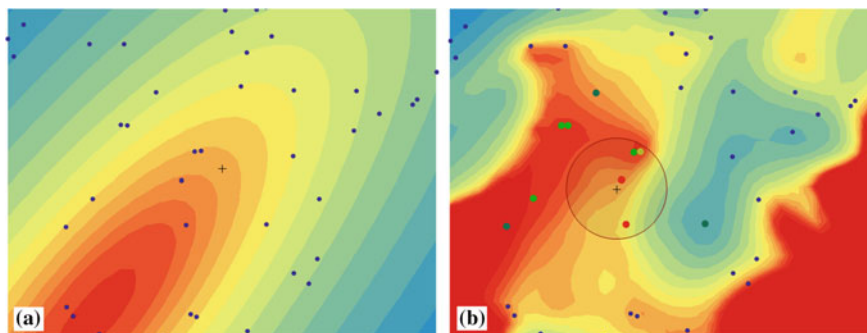


Fig. 2 a Global and b local interpolation methods

Table 1 Spatial interpolation methods (Burrough and McDonnell 1998; Johnston et al. 2001)

| Method | Interpolation type | Local/global | Exact interpolation |
|---------------------------|--------------------|-------------------------|---------------------|
| Global polynomial | Deterministic | Global | No |
| Local polynomial | Deterministic | Local | No |
| Inverse distance weighted | Deterministic | Local | Yes |
| Radial basis functions | Deterministic | Local | Yes |
| Kriging | Geostatistical | Local with global trend | Yes |
| Cokriging | Geostatistical | Local with global trend | Yes |

Table 1 presents a brief summary of the main methods that can be applied in the interpolation of solar radiation data.

The amount of interpolation methods available is quite broad, as well as the parameters susceptible of using for the adjustment in each of them. To calculate solar radiation values, some studies use other variables such as temperature, humidity, cloudiness, precipitation or elevation (Evrendilek and Ertekin 2008; Jolly et al. 2005). Comparative studies have been carried out to establish which is the optimal method for each variable (Apaydin et al. 2004; Vicente-Serrano et al. 2003), although the kriging method is one of the most applied (Antonanzas et al. 2015; Perea-Moreno and Hernandez-Escobedo 2016; Righini et al. 2005).

In order to illustrate the interpolation methods, we provide daily solar radiation data (summer solstice) from 45 radiometric stations in Spain (AEMET 2011) (Fig. 3).



Fig. 3 Distribution of radiometric stations from Spain, located in the Iberian Peninsula

2.1 Deterministic Methods

2.1.1 Global Polynomial Interpolation

When the analyzed parameter varies continuously in a certain area, this interpolation method defines the mathematical function that fits the values of the input sample points. The global polynomial interpolation models a smooth surface that best represents the trend in the data points, in order to differences of observed errors are minimal.

This method uses all data available of the study area to produce a prediction surface. The interpolated values are computed from their geographical location by multiple regressions using a least squares regression fit. The correlation between the variable to interpolate z and its coordinates (x, y) is defined with the function:

$$z(x, y) = \sum_{r+s \leq p} (b_{rs} \cdot x^r \cdot y^s) \quad (1)$$

The number of coefficients b_{rs} to be determined would depend on the order p of the trend surface. First- to third-order polynomial functions are the most common:

$$z(x, y) = b_0 + b_1 \cdot x + b_2 \cdot y \quad (2)$$

$$z(x, y) = b_0 + b_1 \cdot x + b_2 \cdot y + b_3 \cdot x^2 + b_4 \cdot xy + b_5 \cdot y^2 \quad (3)$$

$$z(x, y) = b_0 + b_1 \cdot x + b_2 \cdot y + b_3 \cdot x^2 + b_4 \cdot x \cdot y + b_5 \cdot y^2 + b_6 \cdot x^3 + b_7 \cdot x^2 \cdot y + b_8 \cdot x \cdot y^2 + b_9 \cdot y^3 \quad (4)$$

Being a global interpolation method, it is likely to appear outliers at the edges of the surface, generally related to exceptionally high or low values. The resulting surfaces modeled with low-order polynomials may be suitable to represent certain processes. However, using high-order polynomials, a properly description of the trend surface becomes more complex. In addition, global interpolation is a complementary technique used to identify a general trend that influences on data when a local analysis is implemented.

2.1.2 Local Polynomial Interpolation

With the local polynomial interpolation, instead of using the points of the entire surface, the mathematical function is evaluated exclusively on the surface near each point of estimation. This method fits the function repeatedly to small sections of the sample points, defined by a window, to cover the whole area. The least squares procedure is used by minimizing the expression:

$$\sum_{i=1}^n \omega_i (z(x, y) - \mu_0(x, y))^2 \quad (5)$$

where n is the number of points into the window and the weight ω_i when, for example, the window is a circle is defined as:

$$\omega_i = \left(1 - \frac{d_i}{R}\right)^p \quad (6)$$

where d_i is the distance between the estimated point and a sample point within the window and R is the ratio of the window.

The value of the polynomial $\mu_0(x_i, y_i)$ for first- and second-order functions are:

$$\mu_0(x, y) = b_0 + b_1 \cdot x + b_2 \cdot y \quad (7)$$

$$\mu_0(x, y) = b_0 + b_1 \cdot x + b_2 \cdot y + b_3 \cdot x^2 + b_4 \cdot xy + b_5 \cdot y^2 \quad (8)$$

Local polynomial functions are suitable for evaluating data which have small variations in the nearest region.

2.1.3 Inverse Distance Weighting

Interpolation method based on the premise that considers, the points closest to a location are more similar than those further away. Inverse distance weighting method calculates the value of an unknown point by means of a combining weighted of the values in a sample of points. Using this method, greater weight is given to points located in the nearby position, decreasing their influence as a function of distance. The general formula is the following:

$$\hat{z}(x_0) = \frac{\sum_{i=1}^n \frac{Z(x_i)}{d_{i0}^p}}{\sum_{i=1}^n \frac{1}{d_{i0}^p}} \quad (9)$$

where $\hat{z}(x_0)$ is the figured value for the location x_0 ; n is the number of locations where a value has been measured; d_{i0} represents the distance between the sample locations x_i and the prediction location x_0 ; and, $z(x_i)$ is the value of the location x_i (Slocum et al. 2014).

The power parameter p is the main factor that affecting on the interpolated values, due to it controls assigned weights to the measured points. Weights are proportional to the inverse distance d_{i0} raised to the power p . When the parameter p increases, the weights of the furthest values diminish and nearby points will have a greater influence on the estimated values.

2.1.4 Radial Basis Functions

Radial basis functions are techniques in which the values are determined by different mathematical functions that force the surface to pass through all the measured points. These methods generate continuous flexible surfaces by adjusting the interpolated values to minimize, as much as possible, their total curvature. These functions are quite appropriate when it is necessary to create large smooth surfaces without many variations between an area and the contiguous one.

The interpolated result is defined by a linear combination of the basic functions:

$$\hat{z}(x_0) = \sum_{i=1}^n \omega_i \cdot \phi(r) + \beta \quad (10)$$

where n is the number of sample points; ω_i are weights to be estimated; β is a bias parameter; r is de Euclidean distance between the estimated point and each data location; and, $\phi(r)$ is the radial basis function.

Some of the types of radial basis functions commonly used are:

Thin-plate spline function:

$$\varnothing(r) = (\sigma \cdot r)^2 \cdot \ln(\sigma \cdot r) \quad (11)$$

Multiquadric function:

$$\varnothing(r) = \sqrt{r^2 + \sigma^2} \quad (12)$$

Inverse multiquadric function:

$$\varnothing(r) = \frac{1}{\sqrt{r^2 + \sigma^2}} \quad (13)$$

Spline with tension function:

$$\varnothing(r) = \ln\left(\sigma \cdot \frac{r}{2}\right) + K_0(\sigma \cdot r) + C_E \quad (14)$$

Completely regularized spline function (with tension and smoothing):

$$\varnothing(r) = -\left[\ln\left(\sigma \cdot \frac{r}{2}\right)^2 + E_1\left(\sigma \cdot \frac{r}{2}\right)^2 + C_E\right] \quad (15)$$

The parameter σ controls the smoothness of the function: K_0 is the modified Bessel function (Abramowitz and Stegun 1974); C_E is the Euler constant; and, E_1 is the exponential integral function (Mitášová and Mitáš 1993) (Fig. 4).

2.2 Geostatistical Methods

2.2.1 Kriging

Kriging interpolation methods are characterized by creating a surface applying statistical models and providing information about the accuracy of the results, including the spatial correlation of the data. They are based on the weighted average calculation of the sample measurements. The weights are defined with the distance between the measured points and the location of the prediction, in addition to the spatial structure of the sample points (Slocum et al. 2014).

The kriging procedure consists first, in examining the spatial distribution of the data (autocorrelation) and next, generating the interpolation surface with the most appropriate estimation method.

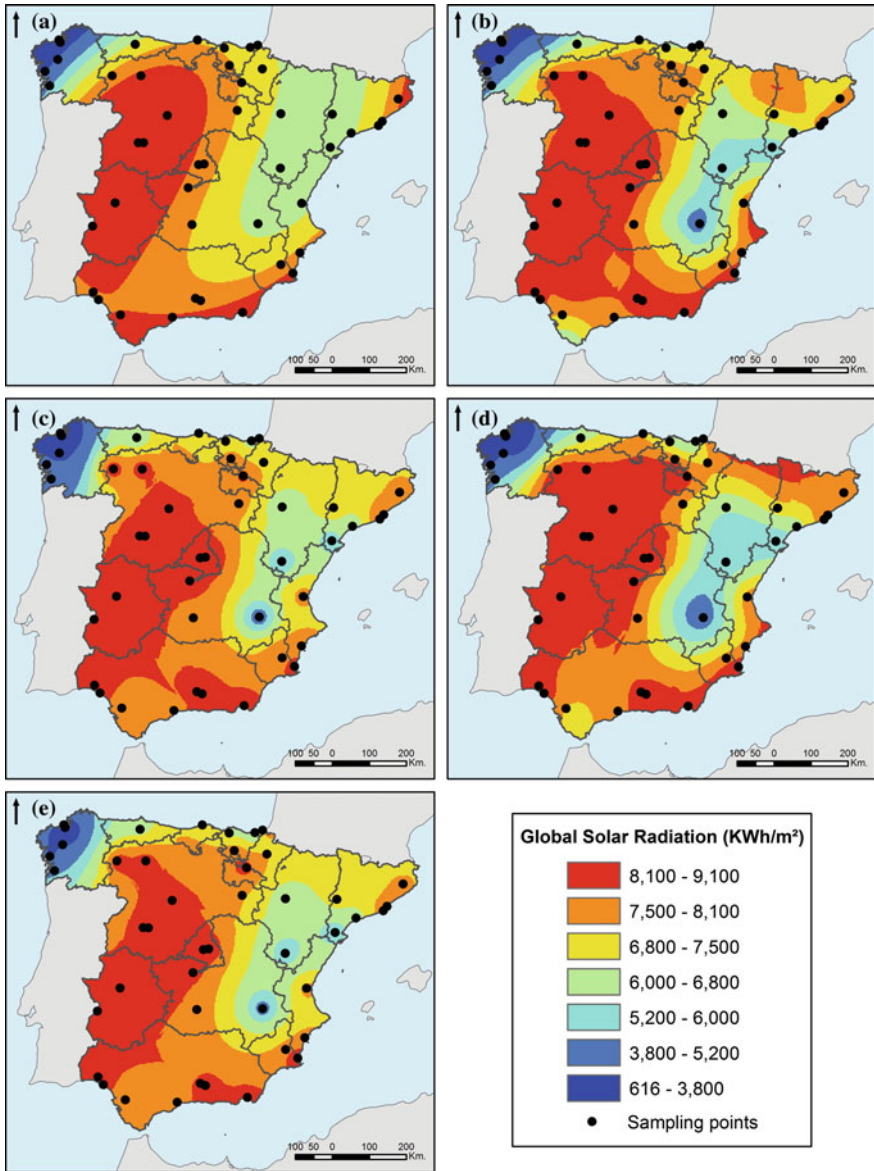


Fig. 4 Estimated global solar radiation for summer solstice (2011) from 45 stations in Spain. Deterministic interpolation methods: **a** global polynomial; **b** local polynomial; **c** inverse distance weighted; **d** thin-plane spline function; and, **e** completely regularized spline function

Autocorrelation

Spatial autocorrelation is analyzed by variance, represented graphically with the variogram, where the spatial variability of a phenomenon is shown according to the sampling points are further away. Semivariance $\gamma(h)$ can be estimated using:

$$\gamma(h) = \frac{1}{2 \cdot n} \sum_{i=1}^n [z(x_i) - z(x_i + h)]^2 \tag{16}$$

where n is the number of sample points separated by a distance interval h ; $z(x_i)$ is the sample value in a location x_i ; and, $z(x_i + h)$ is the value at a distance h from x_i (Burrough and McDonnell 1998).

However, to quantify the scale of spatial variation, it is necessary to adjust the variogram to a theoretical function. This may help to the extraction of a series of parameters which will be used in the kriging interpolation.

In the graph of the variogram (Fig. 5), the variance versus distance is represented. When the distance between points is zero, the semivariance should be zero, but the curve at this point has a value close to zero. This unexplained semivariance is the *nugget* effect, and it indicates measurement errors and variability at a lower scale than the sample. At high values of distance, there is a point at which the semivariance between pairs of points does not increase. The distance at which the semivariance levels off is the *range* and the *sill* is the height reached by the variogram at that point.

The equations of the models to adjust the semivariance are summarized in Table 2.

Types of kriging methods

In general, the predictions of the model for the variable in a location are variants of the equation:

$$\hat{Z}(x_0) - \mu = \sum_{i=1}^n \lambda_i [Z(x_i) - \mu(s_0)] \tag{21}$$

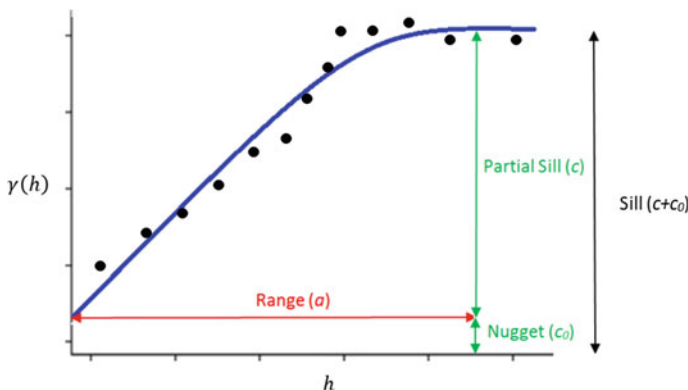
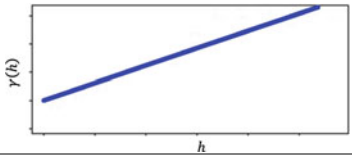
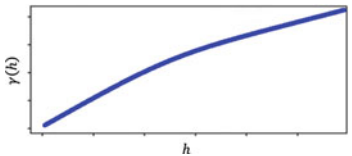
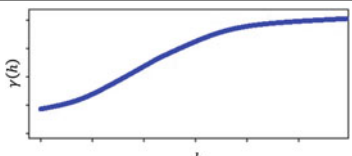
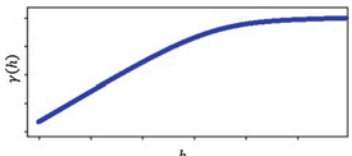


Fig. 5 Example of variogram

Table 2 Semivariance models (Burrough and McDonnell 1998)

| Model | Equations | |
|--------------------------------------------------------------------------------------------------|-------------------------------------------------------------------------------------------------------------------------------------------------------------------|------|
| Linear  | $\gamma(h) = c_0 + b \cdot h$ (b is the slope of the line) | (17) |
| Exponential  | $\gamma(h) = c_0 + c \cdot \left(1 - \exp\left(-\frac{h}{a}\right)\right)$ | (18) |
| Gaussian  | $\gamma(h) = c_0 + c \cdot \left(1 - \exp\left(-\frac{h^2}{a^2}\right)\right)$ | (19) |
| Spherical  | $\gamma(h) = \begin{cases} c_0 + c \cdot \left(\frac{3h}{2a} - \frac{1}{2} \cdot \left(\frac{h}{a}\right)^3\right) & 0 < h < a \\ c_0 + c & h \geq a \end{cases}$ | (20) |

where μ is a known stationary mean value; n is the number of point for the estimation; λ_i is the kriging weight; and $\mu(x_0)$ is the mean of sample data in the search window.

To carry out a prediction when mapping variables, there are different types of kriging methods that can be divided into linear and nonlinear (Cressie 2015; Chilès and Delfiner 2012; Goovaerts 1997; Wackernagel 2003):

Linear methods: The estimates are weighted linear combinations of the data.

- *Ordinary kriging* is the most general and widely used kriging methods. The estimated points are allocated values with a weighted linear combination using sample values. The method assumes that the mean value is constant and unknown over the search neighborhood.
- *Simple kriging* uses the average of the total set of data. It considers the premise that both, the mean value and the semivariance of the process, are known and remain constant in all locations.

- *Universal kriging* is a method that performs the estimation of the variable in the presence of a trend or drift. The analyzed phenomenon consists of a deterministic component and the corresponding residue. The variable is determined as the sum of the deterministic function of the drift and a random function with zero mean, which represents the fluctuation or residual error.

Nonlinear methods: The estimates depend on the statistical distribution of the variables.

- *Indicator kriging* is a method in which continuous data are transformed to a binary scale. A binary indicator variable is obtained by establishing a threshold and assigning value 1 to those that are less or equal than it and 0 to the others. In the resulting interpolation, the distribution of the data will reflect being in a class, depending on whether the data exceeds or falls below the specified threshold.
- *Probability kriging* is a technique based on indicator kriging that uses binary data (0 or 1) and then, applies cokriging to perform a better estimation of the resulted probability. The indicator values are used as the primary variable and the original sample data as the secondary one in the cokriging.
- *Disjunctive kriging* is also a nonlinear method in which the global distributions of the data are normalized by Hermite polynomials. The estimate of the variable is developed with a linear combination of the estimated polynomial values. In addition, this method estimates the probability that a random variable shows of exceeding, or not exceeding, a predetermined level in the analyzed area.

2.2.2 Cokriging

Sometimes the phenomena analyzed depend on the values of an analyzed variable, but other times several phenomena are related to each other. Cokriging offers the option of identifying the characteristics of a primary variable from the data of another variable. This method considers secondary information that can be obtained about the variable investigated, referring to other attributes related to the main one (Goovaerts 1997). The general equation that shows the estimated interpolation of the combination between the primary and secondary variables is:

$$\hat{Z}_1(x_0) - \mu_1 = \sum_{i=1}^{n_1} \lambda_{i1} [Z_1(x_{i1}) - \mu_1(x_{i1})] + \sum_{j=2}^{n_v} \sum_{i_j=1}^{n_j} \lambda_{ij} [Z_j(x_{ij}) - \mu_j(x_{ij})] \quad (22)$$

where μ_1 is a known stationary mean value of the primary variable; n_1 is the number of points for the estimation in the search window; λ_{i1} is the weight of the primary variable; $Z_1(x_{i1})$ is the data of primary variable; $\mu_1(x_{i1})$ is the mean of sampled data in the search window; n_v is the number of secondary variables; n_j number of j secondary variable in the search window; λ_{ij} is the weight of secondary variable;

$Z_j(x_{ij})$ is the data of secondary variable; and, $\mu_j(x_{ij})$ is the mean of sample secondary variable in the search window.

In cokriging, the spatial dependency relationships are specified by the autocorrelation of the different variables and the cross-correlation between the data. To define the coherence between the variables, a crossed variogram is elaborated, where the variance represented will no longer be between points of the same variable, but between the values of one variable in relation to the other. To verify that there is a covariation, between the primary and secondary variable, a semi-variogram can be estimated from the following equation:

$$\gamma_{12} = \frac{1}{2 \cdot n} \sum_{i=1}^n [z_1(x_i) - z_1(x_i + h)] \cdot [z_2(x_i) - z_2(x_i + h)] \quad (23)$$

where n is the number of pairs of sampled points of variable z_1 and z_2 in locations x_i and $x_i + h$ separated by a distance h (Burrough and McDonnell 1998).

There are several cokriging methods that include ordinary cokriging, simple cokriging, universal cokriging, indicator cokriging, probability cokriging and disjunctive cokriging (Cressie 2015; Chilès and Delfiner 2012; Goovaerts 1997; Isaaks and Srivastava 1989) (Fig. 6) (Table 3).

3 Modeling Solar Radiation Using GIS

When the objective is to determine more precisely the distribution of the incident solar radiation in a region or a specific location, establishing a single value for an area that is too wide may be insufficient. At regional and local scales, altitude, orientation, slope, and shading can generate microclimates and, a more or less homogeneous distribution of solar radiation. In these cases, the topography of the area helps to incorporate these factors into the analysis, improving the estimation of solar radiation when the variations caused by the terrain effect are considered.

There are different GIS software packages that have models for estimating solar radiation. The r.sun model designed for the free software GRASS GIS (GRASS Development Team 2018) calculates the three components of solar radiation (direct, diffuse and reflected) with clear sky conditions. It incorporates the possibility of including the effect of shading due to topography and a cloud attenuation factor (Hofierka et al. 2007; Šúri and Hofierka 2004).

In addition, the models developed for the ArcGIS software by ESRI (Environmental Systems Research Institute) (Esri 2018), provided the tool 'Area Solar Radiation' available with the extension 'Spatial Analyst'. This tool of ArcGIS represents and analyzes the insolation for a period of time in a geographical area that is represented by terrain raster file (Digital Surface Model—DSM). The analysis result is the global solar radiation for each location of a surface and is calculated as the addition of the direct and diffuse solar radiation (Esri 2017a). It is

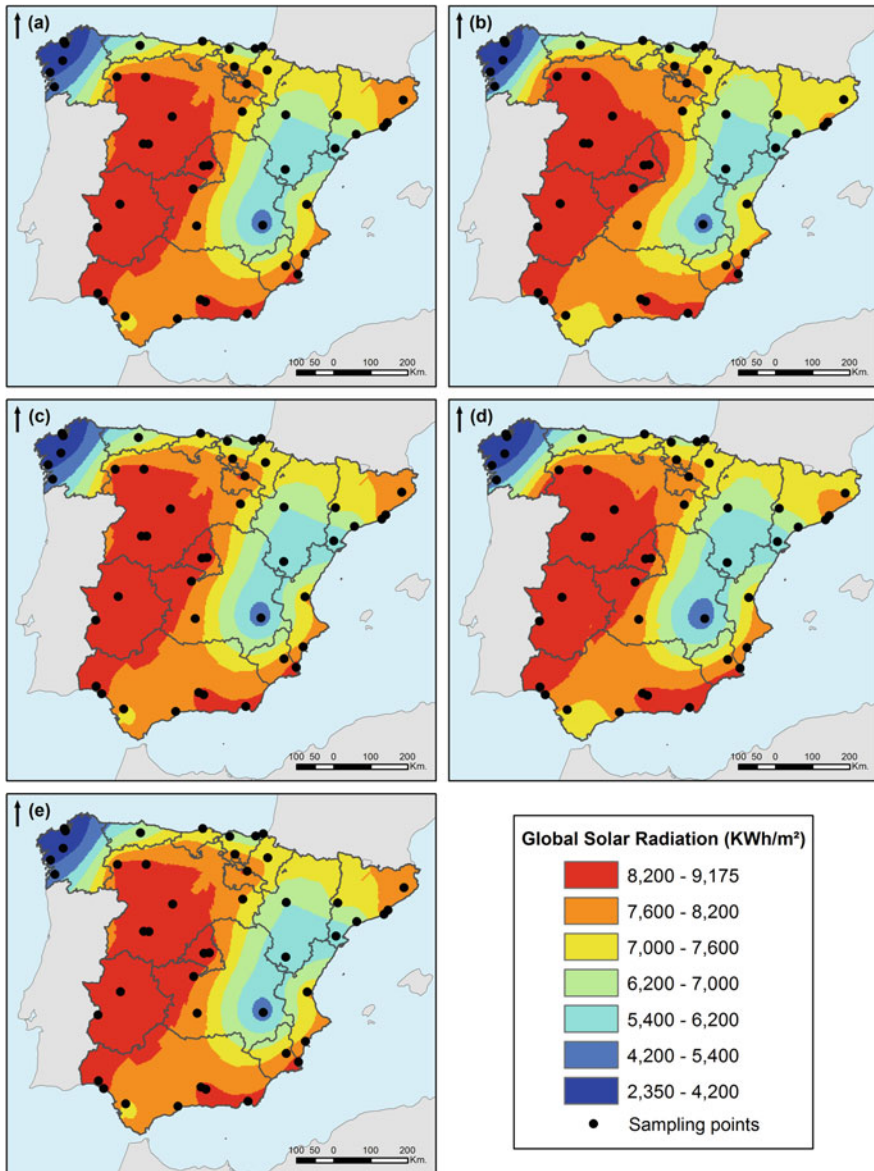


Fig. 6 Estimated global solar radiation for summer solstice (2011) from 45 stations in Spain. Geostatistical interpolation methods: **a** ordinary kriging; **b** simple kriging; **c** universal kriging; **d** disjunctive kriging; and, **e** ordinary cokriging

designed to work on local scales because it only defines a latitude value for the entire area. It can also be used for national and continental scales if the input DSM is divided into small areas (Fig. 7).

Table 3 Errors statistic of the prediction values of global solar radiation interpolation (summer solstice of 2011) from 45 stations in Spain

| Interpolation method | ME | RMAE | MSE | RMSSE | ASE |
|----------------------------------------|-------|--------|---------|-------|--------|
| Global polynomial | 10.26 | 727.53 | – | – | – |
| Local polynomial | 71.28 | 790.75 | – | – | – |
| Inverse distance weighted | 17.23 | 820.78 | – | – | – |
| Thin-plate spline function | 5.34 | 829.69 | – | – | – |
| Completely regularized spline function | 2.52 | 774.18 | – | – | – |
| Ordinary kriging | 13.85 | 759.95 | 0.004 | 0.98 | 793.58 |
| Simple kriging | 5.38 | 763.89 | 0.006 | 0.93 | 841.38 |
| Universal kriging | 14.09 | 759.88 | 0.004 | 1.003 | 783.74 |
| Disjunctive kriging | 18.05 | 752.12 | 0.008 | 0.87 | 821.30 |
| Ordinary cokriging | 9.63 | 782.54 | 0.00004 | 1.02 | 777.97 |

ME Mean Error, RMSE Root Mean Square Error, MSE Mean Standardized Error, RMSSE Root Mean Square Standardized Error, ASE Average Standard Error (*Mean Error* (ME) shows the average difference value between the measured data and the prediction. *Root Mean Square Error* (RMSE) indicates the grade of bias from the predictions with the measured values. The smaller this error, the prediction is better. *Mean Standardized Error* (MSE) is the average of the standardized error whose value should be nearby 0. *Root Mean Square Standardized Error* (RMSSE) should be close to 1. If the error is greater than 1, the prediction is underestimated and if the error is less than 1, the prediction is overestimated. *Average Standard Error* (ASE) is the mean of the prediction standard error.) (Esri 2017b)

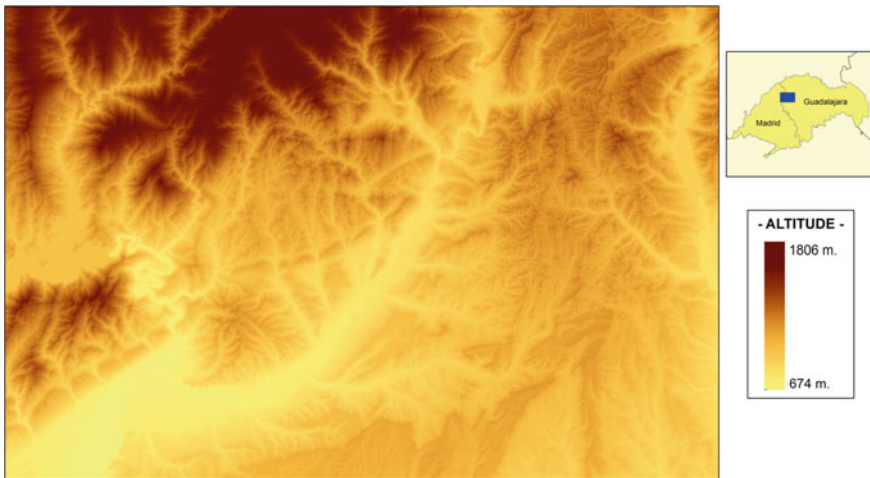


Fig. 7 Digital surface model (pixel 25 m). Area of Guadalajara and Madrid provinces (Spain). Coordinates: 40° 51' 59.56"N, 3° 21' 15.18"O (IGN 2015)

3.1 Calculation of Solar Radiation with ArcGIS

‘Area Solar Radiation’ tool is based on algorithms developed by Fu and Rich (1999) that determine the hemispheric viewshed, the sunmap and the skymap that calculate the amount of solar radiation on a location:

1. The *viewshed* shows, by searching in a series of directions, those areas of the sky that are visible or hidden due to topography or nearby structures, when they are observed from a certain point.
In the raster representation of the viewshed, each cell is assigned a value relative to the visibility of the direction of the sky and its location (row and column) is represented for the zenith and azimuth angles.
2. The *sunmap* determines the way of the Sun in the sky over a period of time. In the resulting raster map, the apparent position of the Sun is calculated with the latitude of the area, and it is represented with intervals that vary during the periods of the day (hours) and of the year (days or months). Each sector of the sunmap is assigned an identifying value together with the zenith and azimuthal angles.
3. A *skymap* consists of the division of the sky into a series of sectors in which diffuse radiation can be originated. The sectors that shape the map of the sky are also assigned an identifying value. They defined by the zenith and azimuthal angles, which calculate the diffuse solar radiation in each sky sector (Fig. 8).

Then viewshed is overlaid with the sunmap and the skymap to calculate, respectively, the direct and diffuse solar radiation that are originated from each direction of the sky (Esri 2017a; Kodysh et al. 2013) (Fig. 9).

Analyzing solar radiation in a specific area requires taking into account factors that are responsible for attenuating the amount of radiation that finally reaches the surface. Topography, atmospheric agents, and seasonal variation of insolation are major factors that affect the spatial distribution of solar radiation.

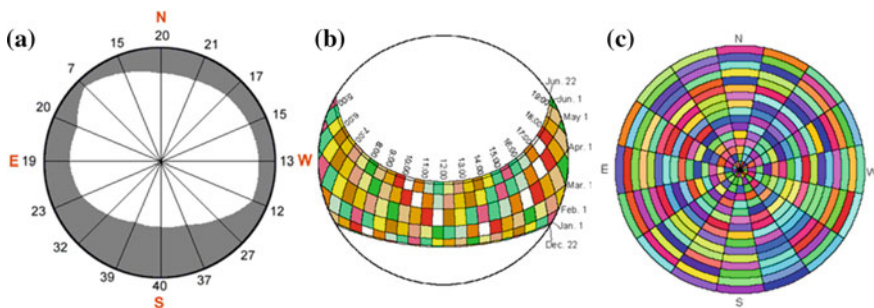


Fig. 8 a Viewshed, b sunmap for winter to summer solstices y c a skymap with sky sectors defined by 16 zenith and azimuth divisions (Fu and Rich 2000)

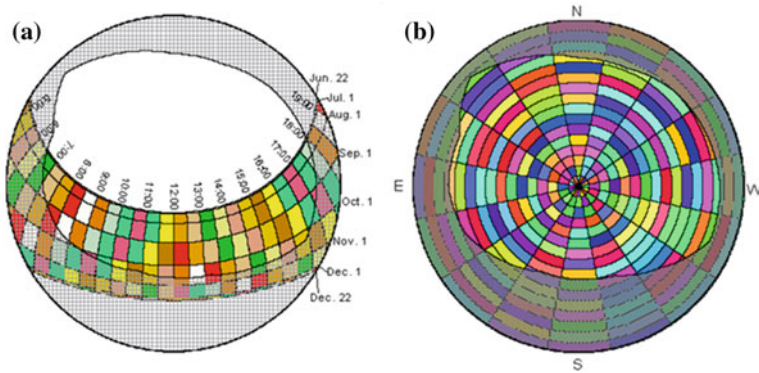


Fig. 9 **a** Overlay of viewshed with sunmap y **b** overlay of viewshed with skymap (Fu and Rich 2000)

Shading limits the amount of insolation in a specific location and the characteristics of the surfaces, their slope, and orientation determine the angle of incidence of solar radiation. In addition, the weather conditions and the effect of the atmosphere also influence the attenuation of the final values of insolation. These factors are considered by estimating atmospheric transparency (transmissivity) and diffuse proportion of solar radiation.

'Area Solar Radiation' tool has options to establish parameters to fit the variables that define the study area and influence on the insolation levels. The inclusion of atmospheric parameters to adjust the calculation of solar radiation with ArcGIS can be done using different methodologies. Sun et al. (2013) apply an annual value for these factors. However, other studies use monthly data provide by agencies such as NASA or the PVGIS databases (Brito et al. 2012; Fogl and Moudrý 2016), which adapt the results better to the monthly and seasonal variations of the solar radiation. Cloud coverage data from meteorological stations and weather databases are also utilized in the parameter calculation for ArcGIS (Oloo et al. 2015; Wong et al. 2016).

Some works use models to calibrate and obtain adequate data for each month of the year. With the solar radiation values get in different measuring stations, Tooke et al. (2011) determine the atmospheric transparency index, from which the diffuse proportion derives, using a first-order model proposed by Orgill and Hollands (1977). Mavromatidis et al. (2015) calculate the global radiation for all possible combinations of transmissivity and diffuse proportion, selecting a set of monthly values that give a result closer to the values calculated with the Meteororm software (Meteotest 2017).

We propose to estimate the monthly values of atmospheric parameters, using a reference day for each month of the year and the horizontal radiation data of a location. First, analytically the transmissivity is determined and subsequently the diffuse proportion is derived with a linear correlation. To show the temporal variation of the insolation, global solar radiation map is calculated for all the months of

the year and then, adds the results of the twelve maps to obtain the total annual value (Figs. 10 and 11).

3.1.1 Transmissivity

Transmittivity is the proportion of the solar radiation that goes through the atmosphere and reaches the surface of the Earth with respect to the solar radiation received outside the atmosphere (extraterrestrial). The values that this parameter can take values between 0 (without transmission) and 1 (complete transmission), considering that a value of 0.5 corresponds to a generally clear sky.

To establish the monthly transmissivity values, the monthly average clearness index K_T is calculated. This parameter is defined as the ratio between is the monthly average daily radiation on a horizontal surface H_h and the extraterrestrial solar radiation incident on a horizontal plane H_0 :

$$K_T = H_h/H_0 \tag{24}$$

The global radiation on a horizontal surface values H_h for each month is obtained from the PVGIS database by selecting a location on the interactive map (European Commission 2012).

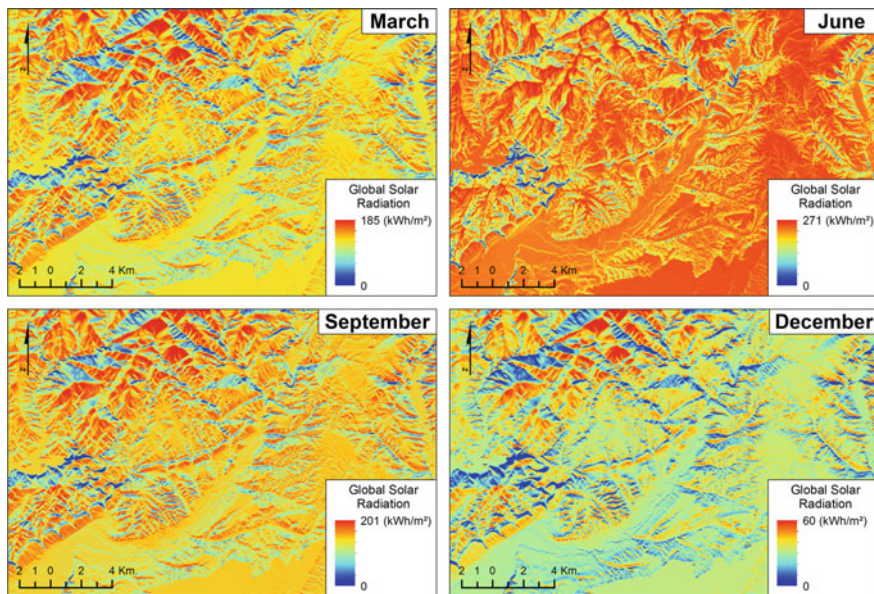


Fig. 10 Global solar radiation for some months (March, June, September, and December). Area of Guadalajara and Madrid provinces (Spain)

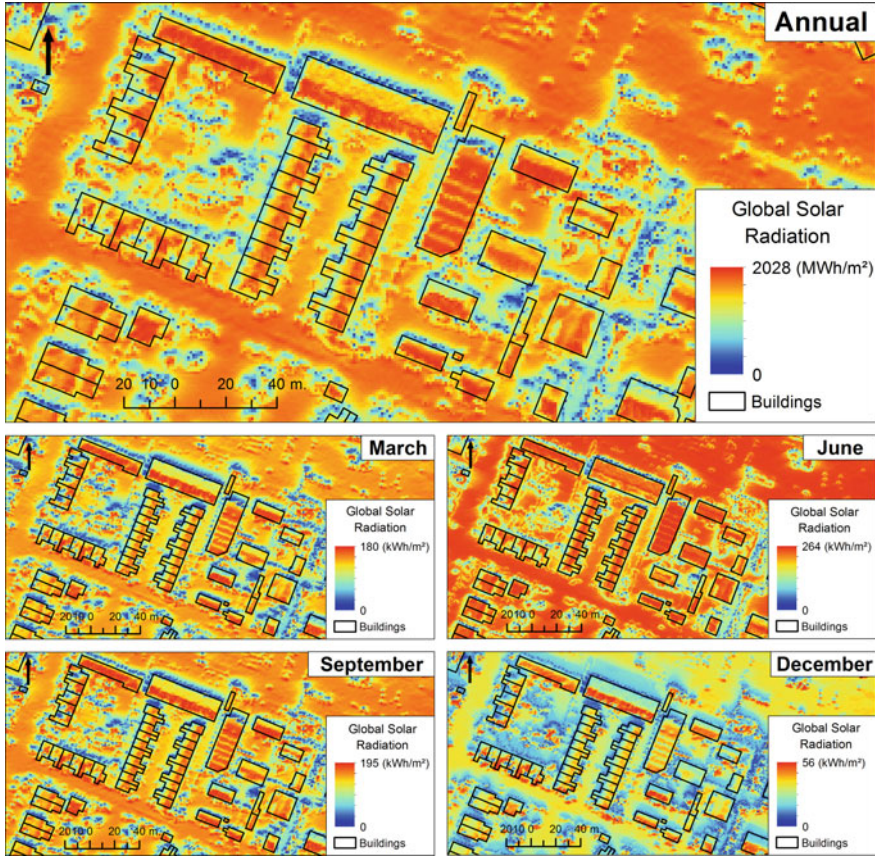


Fig. 11 Global solar radiation for some months (March, June, September, and December) and annual. Set of buildings in the town of Alpedrete (Madrid)

Analytically, the extraterrestrial solar radiation incident on a horizontal plane H_0 can be calculated by the expression:

$$H_0 = (24/\pi) \cdot I_{SC} \cdot [1 + 0.033 \cdot (360 \cdot n/365)] \cdot [\cos \phi \cdot \cos \delta \cdot \sin \omega_s + (\pi \cdot \omega_s/180) \cdot \sin \phi \cdot \sin \delta] \tag{25}$$

where I_{SC} is the solar constant (1367 W/m² day); n is the selected day for each month (Table 4); and, ϕ is the latitude.

There are different approaches for the determination of declination angle δ . According to the equation of Cooper (1969), for a Julian day n of year, the declination is expressed as:

Table 4 Recommended average day for each month (Klein 1977)

| Month | Day of the year | Date | Month | Day of the year | Date |
|----------|-----------------|---------|-----------|-----------------|---------|
| January | 17 | 17 Jan. | July | 198 | 17 Jul. |
| February | 47 | 16 Feb. | August | 228 | 16 Aug. |
| March | 75 | 16 Mar. | September | 258 | 15 Sep. |
| April | 105 | 15 Apr. | October | 288 | 15 Oct. |
| May | 135 | 15 May. | November | 318 | 14 Nov. |
| June | 162 | 11 Jun. | December | 344 | 10 Dec. |

$$\delta = 23.45 \cdot \sin\left(360 \cdot \frac{284 + n}{365}\right) \quad (26)$$

Sunset hour angle ω_s is calculated by the equation (Duffie and Beckman 2013):

$$\cos \omega_s = -\tan \phi \cdot \tan \delta \quad (27)$$

3.1.2 Diffuse Proportion

Diffuse proportion is the fraction of the global solar radiation that is diffuse. The values of this parameter vary from 0 to 1, establishing as a value of 0.3 for generally clear sky conditions.

The coefficient of monthly average diffuse ratio K_D , which represents the relation between the global solar radiation and the diffuse component of the radiation, is calculated to determine the diffuse proportion. This parameter is based on the monthly average clearness index K_T and is calculated using the correlation of Gopinathan and Soler (1995) (Table 5).

$$K_D = 0.91138 - 0.6225 \cdot K_T \quad (28)$$

Table 5 Values of transmissivity and diffuse proportion

| Month | H_b (Wh/m ²) | Transmissivity | Diffuse proportion |
|-----------|----------------------------|----------------|--------------------|
| January | 1930 | 0.45 | 0.47 |
| February | 2980 | 0.39 | 0.54 |
| March | 4430 | 0.34 | 0.59 |
| April | 5260 | 0.38 | 0.55 |
| May | 6330 | 0.36 | 0.57 |
| June | 7430 | 0.29 | 0.64 |
| July | 7800 | 0.25 | 0.69 |
| August | 6710 | 0.27 | 0.66 |
| September | 5090 | 0.32 | 0.62 |
| October | 3510 | 0.36 | 0.57 |
| November | 2230 | 0.42 | 0.50 |
| December | 1770 | 0.45 | 0.48 |

Area of Guadalajara and Madrid provinces (Spain)

4 Conclusions

The purpose of this chapter has been to describe some of the available options for estimating the distribution of solar radiation in geographic areas. Several methods of interpolation and approximation were developed to predict the values of a spatial phenomenon in a location. In the interpolation examples shown previously, although the polynomial global method has the smallest root mean quadratic error that results in interpolations closer to the real value, it is observed that the geo-statistical methods, in general show very low quadratic errors. Within this group, the universal kriging and ordinary Cokriging methods are the ones that show the greatest adjustment in the results. The mean standardized error close to 0 and the root mean square standardized error nearby 1 (Table 3).

Although all interpolation techniques are valid, it is important to analyze whether the interpolation method and the selected criteria are the most appropriate. A method that conforms well to a data set may not be the most appropriate for a different data set. The application of each method will consider the objective of the interpolation, the properties of the available data and the distribution of the sample.

Sometimes, there are not enough measurement points or the solar radiation distribution changes on a very short spatial scale, such as mountainous regions or urban areas with a complex morphology. An alternative to interpolation procedures are the modeling techniques developed for GIS software that manage large amounts of geo-referenced data. Models for estimating solar radiation are mainly based on a three-dimensional surface model and, using a series of zonal parameters, they are adjusted as much as possible to the characteristics of the geographical area under study.

GIS analysis tools for the prediction and mapping of the solar resource are increasingly powerful. The objective is to highlight the potential presented by this type of tools for the representation of this phenomenon without forgetting the purpose of carrying out a specific study. Users will have to choose the technology that best suits each one and analyze the results according to the method and parameters that defines it.

References

- Abramowitz M, Stegun IA (1974) Handbook of mathematical functions, with formulas, graphs, and mathematical tables. Dover Publications Inc, New York
- Agencia Estatal de Meteorología AEMET (2011) Agencia Estatal de Meteorología. <http://www.aemet.es/es/portada>. Accessed 29 Mar 2018
- Antonanzas J, Urraca R, Martínez-de-Pison FJ, Antonanzas-Torres F (2015) Solar irradiation mapping with exogenous data from support vector regression machines estimations. *Energy Convers Manage* 100:380–390. <https://doi.org/10.1016/j.enconman.2015.05.028>
- Apaydin H, Kemal SF, Yildirim YE (2004) Spatial interpolation techniques for climate data in the GAP region in Turkey. *Clim Res* 28:31–40
- Brito MC, Gomes N, Santos T, Tenedório JA (2012) Photovoltaic potential in a Lisbon suburb using LiDAR data. *Sol Energy* 86:283–288
- Burrough PA, McDonnell RA (1998) Principles of geographical information systems. Oxford University Press, Oxford
- Chilès J-P, Delfiner P (2012) Geostatistics: modeling spatial uncertainty. Willey Series in Probability and Statistics. Wiley, Hoboken
- Cooper PI (1969) The absorption of radiation in solar stills. *Sol Energy* 12:333–346. [https://doi.org/10.1016/0038-092X\(69\)90047-4](https://doi.org/10.1016/0038-092X(69)90047-4)
- Cressie N (2015) Statistics for spatial data, revised edition. Wiley Classic Library. Wiley, Hoboken
- Duffie JA, Beckman WA (2013) Solar engineering of thermal processes. Wiley-Interscience, Hoboken
- Esri (2017a) ArcGIS desktop. Tools: an overview of the solar radiation toolset. <http://desktop.arcgis.com/en/arcmap/10.3/tools/spatial-analyst-toolbox/an-overview-of-the-spatial-analyst-toolbox.htm>. Accessed 29 Mar 2018
- Esri (2017b) ArcGIS Pro. Tool reference: cross validation. <https://pro.arcgis.com/en/pro-app/tool-reference/geostatistical-analyst/cross-validation.htm>. Accessed 29 Mar 2018
- Esri (2018) Esri: GIS mapping software, spatial data analytics and location platform. <https://www.esri.com/es-es/home>. Accessed 29 Mar 2018
- European Commission (2012) Photovoltaic geographical information system interactive maps (PVGIS). <http://re.jrc.ec.europa.eu/pvgis/apps4/pvest.php?lang=es&map=europe>. Accessed 29 Mar 2018
- Evrindik F, Ertekin C (2008) Assessing solar radiation models using multiple variables over Turkey. *Clim Dyn* 31:131–149. <https://doi.org/10.1007/s00382-007-0338-6>
- Fogl M, Moudry V (2016) Influence of vegetation canopies on solar potential in urban environments. *Appl Geogr* 66:73–80. <https://doi.org/10.1016/j.apgeog.2015.11.011>
- Fu P, Rich PM (1999) Design and implementation of the solar analyst: an ArcView extension for modeling solar radiation at landscape scales. In: Proceedings of the 19th annual ESRI user conference, San Diego, USA
- Fu P, Rich PM (2000) The solar analyst 1.0 user manual. Helios Environmental Modeling Institute (HEMI), USA
- Goovaerts P (1997) Geostatistics for natural resources evaluation. Applied geostatistics series. Oxford University Press, New York

- Gopinathan KK, Soler A (1995) Diffuse radiation models and monthly-average, daily, diffuse data for a wide latitude range. *Energy* 20:657–667. [https://doi.org/10.1016/0360-5442\(95\)00004-Z](https://doi.org/10.1016/0360-5442(95)00004-Z)
- GRASS Development Team (2018) GRASS GIS. <https://grass.osgeo.org/>. Accessed 29 Mar 2018
- Hofierka J, Šúri M, Huld T (2007) r.sun. Solar irradiance and irradiation model. <https://grass.osgeo.org/grass75/manuals/r.sun.html>. Accessed 29 Mar 2018
- Instituto Geográfico Nacional IGN (2015) Modelos Digital del Terreno - MDT25. Hoja MTN50 0485. <http://www.ign.es/web/ign/portal>. Accessed 29 Mar 2018
- Isaaks EH, Srivastava RM (1989) An introduction to applied geostatistics. Oxford University Press, New York
- Johnston K, Ver Hoef JM, Krivoruchko K, Lucas N (2001) ArcGIS 9. Using ArcGIS geostatistical analyst. ESRI, Redlands, CA, USA
- Jolly WM, Graham JM, Michaelis A, Nemani R, Running SW (2005) A flexible, integrated system for generating meteorological surfaces derived from point sources across multiple geographic scales. *Environ Model Softw* 20:873–882
- Klein SA (1977) Calculation of monthly average insolation on tilted surfaces. *Sol Energy* 19:325–329. [https://doi.org/10.1016/0038-092X\(77\)90001-9](https://doi.org/10.1016/0038-092X(77)90001-9)
- Kodysh JB, Omitaomu OA, Bhaduri BL, Neish BS (2013) Methodology for estimating solar potential on multiple building rooftops for photovoltaic systems. *Sustain Cities Soc* 8:31–41
- Mavromatidis G, Orehounig K, Carmeliet J (2015) Evaluation of photovoltaic integration potential in a village. *Sol Energy* 121:152–168. <https://doi.org/10.1016/j.solener.2015.03.044>
- Meteotest (2017) Meteonorm. Global irradiation and climate data. <https://meteotest.ch/en/>. Accessed 29 Mar 2018
- Mitášová H, Mitáš L (1993) Interpolation by regularized spline with tension: I. Theory and implementation. *Math Geol* 25:641–655. <https://doi.org/10.1007/BF00893171>
- Oloo FO, Olang L, Strobl J (2015) Spatial modelling of solar energy potential in Kenya. *Int J Sustain Energy Plann Manage* 6:17–30. <https://doi.org/10.5278/ijsepm.2015.6.3>
- Orgill JF, Hollands KGT (1977) Correlation equation for hourly diffuse radiation on a horizontal surface. *Sol Energy* 19:357–359. [https://doi.org/10.1016/0038-092X\(77\)90006-8](https://doi.org/10.1016/0038-092X(77)90006-8)
- Perea-Moreno A-J, Hernandez-Escobedo Q (2016) Solar resource for urban communities in the Baja California Peninsula, Mexico. *Energies* 9 <https://doi.org/10.3390/en9110911>
- Righini R, Grossi Gallegos H, Raichijk C (2005) Approach to drawing new global solar irradiation contour maps for Argentina. *Renew Energy* 30:1241–1255. <https://doi.org/10.1016/j.renene.2004.10.010>
- Santos Preciado JM, García Lázaro FJ (2008) Análisis estadístico de la información geográfica. Cuadernos UNED. Universidad Nacional de Educación a Distancia, UNED, Madrid
- Slocum TA, McMaster RB, Kessler FC, Howard HH (2014) Thematic cartography and geovisualization: pearson new international edition. Thematic cartography and geovisualization. Pearson Education Limited, London
- Sun YW, Hof A, Wang R, Liu J, Lin YJ, Yang DW (2013) GIS-based approach for potential analysis of solar PV generation at the regional scale: a case study of Fujian Province. *Energy Policy* 58:248–259
- Šúri M, Hofierka J (2004) A new GIS-based solar radiation model and its application to photovoltaic assessments. *Trans GIS* 8:175–190. <https://doi.org/10.1111/j.1467-9671.2004.00174.x>
- Tooke TR, Coops NC, Voogt JA, Meitner MJ (2011) Tree structure influences on rooftop-received solar radiation. *Landscape Urban Planning* 102:73–81
- Vicente-Serrano SM, Saz-Sánchez MA, Cuadrat JM (2003) Comparative analysis of interpolation methods in the middle Ebro Valley (Spain): application to annual precipitation and temperature. *Climate Res* 24:161–180
- Wackernagel H (2003) Multivariate geostatistics: an introduction with applications. Springer, Berlin
- Wong MS et al (2016) Estimation of Hong Kong's solar energy potential using GIS and remote sensing technologies. *Renew Energy* 99:325–335. <https://doi.org/10.1016/j.renene.2016.07.003>